



# A Comparison of Three Methods for Measuring Distortion in Optical Windows

*Robert C. Youngquist*  
*NASA, Kennedy Space Center, Florida*

*Mark A. Nurge*  
*NASA, Kennedy Space Center, Florida*

*Miles Skow*  
*NASA, Kennedy Space Center, Florida*

## NASA STI Program...in Profile

Since its founding, NASA has been dedicated to the advancement of aeronautics and space science. The NASA Scientific and Technical Information (STI) program plays a key part in helping NASA maintain this important role.

The NASA STI Program operates under the auspices of the Agency Chief Information Officer. It collects, organizes, provides for archiving, and disseminates NASA's STI. The NASA STI program provides access to the NASA Aeronautics and Space Database and its public interface, the NASA Technical Reports Server, thus providing one of the largest collections of aeronautical and space science STI in the world. Results are published in both non-NASA channels and by NASA in the NASA STI Report Series, which includes the following report types:

- **TECHNICAL PUBLICATION.** Reports of completed research or a major significant phase of research that present the results of NASA programs and include extensive data or theoretical analysis. Includes compilations of significant scientific and technical data and information deemed to be of continuing reference value. NASA counterpart of peer-reviewed formal professional papers but has less stringent limitations on manuscript length and extent of graphic presentations.
- **TECHNICAL MEMORANDUM.** Scientific and technical findings that are preliminary or of specialized interest, e.g., quick release reports, working papers, and bibliographies that contain minimal annotation. Does not contain extensive analysis.
- **CONTRACTOR REPORT.** Scientific and technical findings by NASA-sponsored contractors and grantees.
- **CONFERENCE PUBLICATION.** Collected papers from scientific and technical conferences, symposia, seminars, or other meetings sponsored or cosponsored by NASA.
- **SPECIAL PUBLICATIONS.** Scientific, technical, or historical information from NASA programs, projects, and missions, often concerned with subjects having substantial public interest.
- **TECHNICAL TRANSLATION.** English-language translations of foreign scientific and technical material pertinent to NASA's mission.

Specialized services also include creating custom thesauri, building customized databases, organizing and publishing research results.

For more information about the NASA STI program, see the following:

- Access the NASA STI program home page at <http://www.sti.nasa.gov>
- E-mail your question via the Internet to [help@sti.nasa.gov](mailto:help@sti.nasa.gov)
- Fax your question to the NASA STI Help Desk at 443-757-5803
- Telephone the NASA STI Help Desk at 443-757-5802
- Write to:  
NASA Center for Aerospace Information (CASI)  
7115 Standard Drive  
Hanover, MD 21076-1320

NASA/TM—2015—218822



# A Comparison of Three Methods for Measuring Distortion in Optical Windows

*Robert C. Youngquist*  
*NASA, Kennedy Space Center, Florida*

*Mark A. Nurge*  
*NASA, Kennedy Space Center, Florida*

*Miles Skow*  
*NASA, Kennedy Space Center, Florida*

National Aeronautics and  
Space Administration

Kennedy Space Center

---

April 2015

## Acknowledgments

We would like to acknowledge Deborah A. Guelzow and Beverly A. Bush of the Kennedy Space Center Library for literature search and retrieval support.

Available from:

NASA Center for AeroSpace Information  
7115 Standard Drive  
Hanover, MD 21076-1320

National Technical Information Service  
5301 Shawnee Road  
Alexandria, VA 22312

Available in electronic form at <http://www.sti.nasa.gov>.

## Preface

We became interested in optical distortion while developing a capability at the Kennedy Space Center to perform wavefront measurements on window assemblies for spaceflight vehicles. The point of these measurements was to limit the degradation of the imagery seen through vehicle windows to an acceptable level. For this reason, some members of our team referred to this as a distortion measurement while others said that it was not. So we examined the definition of distortion to resolve this disagreement and found that both parties were correct. What we were measuring with our phase-shifting interferometer was the optical path length of a window assembly, and nowhere in the published literature was this associated with distortion. However, after further examination we realized that there was a relationship between the window distortion described in the literature and the optical path length function and that this relationship was not recorded in the literature.

We decided to investigate this relationship and soon found that the prior literature described a distortion measurement method that used moiré interferometry. This intrigued us as well since we had used Schlieren imaging, i.e., moiré interferometry, on many occasions to evaluate optical systems qualitatively, but had never developed the mathematics to perform a quantitative assessment. Now though, with the prior literature available and the mathematical foundations provided by the published distortion definitions and our own phase-shifting interferometry work, we had the tools to connect a form of Schlieren imaging to the measurement of window distortion.

The classical technique for measuring distortion is to compare the image of a test pattern with and without the window present. We proceeded to take a small test window and measure its distortion using these three techniques: image comparison, moiré interferometry, and phase-shifting interferometry. We developed the mathematical analysis needed to convert the measurements obtained to the optical definition of distortion and were thus able to compare these three techniques. After summarizing this work at a conference, we decided to write a NASA Technical Memorandum to provide details on our mathematical analysis for those who might one day need alternative ways to measure window distortion.

This page was intentionally left blank.

## Contents

1	INTRODUCTION .....	1
2	DISTORTION DEFINITIONS.....	2
2.1	Distortion Definition 1 .....	3
2.2	Distortion Definition 2.....	4
2.3	Distortion Definition 3.....	5
2.4	Component and Total Distortion .....	5
3	THE IMAGE COMPARISON METHOD .....	7
3.1	Mathematical Analysis.....	7
3.2	Algorithmic Analysis .....	9
3.3	Results.....	11
4	THE MOIRÉ INTERFEROMETRY METHOD.....	13
4.1	Mathematical Analysis.....	15
4.2	Algorithmic Analysis .....	17
4.3	Results.....	19
5	THE PHASE-SHIFTING INTERFEROMETRY METHOD .....	21
5.1	Mathematical Analysis.....	23
5.2	Algorithmic Analysis .....	24
5.3	Results.....	24
6	CONCLUSIONS.....	27

## Figures

Figure 1. Window Segment with Distortion .....	2
Figure 2. Light Refraction by a Window Segment .....	3
Figure 3. Image Comparison Optical System .....	7
Figure 4. Image Comparison Math 1 .....	8
Figure 5. Image Comparison Math 2 .....	8
Figure 6. The Line Pattern Images.....	10
Figure 7. Line Pattern Processing .....	10
Figure 8. $y$ -direction Angular Deviation .....	11
Figure 9. $x$ -direction Angular Deviation .....	12
Figure 10. Moiré System 1.....	13
Figure 11. Moiré System 2.....	14
Figure 12. Moiré System Line Deflection .....	14
Figure 13. Moiré Math Without Window .....	15
Figure 14. Moiré Math Perfect Window.....	17
Figure 15. Moiré Pattern Lines .....	18
Figure 16. Line Pattern Processing.....	18
Figure 17. Moiré Angular Deviation in $y$ .....	19
Figure 18. Moiré Angular Deviation in $x$ .....	20
Figure 19. Zygo Phase-Shifting Interferometer .....	21
Figure 20. Reference Measurement .....	22
Figure 21. Window Optical Path Length 1 .....	22
Figure 22. Window Optical Path Length 2 .....	23
Figure 23. Phase-Shifting Angular Deviation in $y$ .....	24
Figure 24. Phase-Shifting Angular Deviation in $x$ .....	25
Figure 25. Phase-Shifting Distortion in $y$ .....	26
Figure 26. Phase-Shifting Distortion in $x$ .....	26

## 1 INTRODUCTION

The primary function of a window is to allow observation of a potentially hazardous environment, while at the same time providing protection from that environment. Yet, from the window designer's point of view, protection has almost always taken precedence over image quality—no matter whether the windows are providing protection from wind, rain, uncomfortable temperatures, or airborne debris, or in the case of aircraft and spacecraft, from extreme pressures and temperatures. This bias was most strikingly borne out in a 1981 Air Force report [1] discussing optical distortion requirements that stated “The F-106, F-111, B-1, T-28, F-5, and F-15 have all exceeded these requirements, and sacrificing pilot visual performance has been justified by the increased aerodynamic performance of the aircraft.” Such a design preference is defensible—it is more important to protect an astronaut from the vacuum of space than to provide clear imagery—yet these are not exclusive requirements. Advances in materials and material processing allow the designer to attain better optical performance without sacrificing important material characteristics such as strength. In addition, demand for increased performance of spacecraft windows, which are now used for photography and telescope observations, and even for laser communications, requires giving greater consideration to optical clarity.

Along with the need for better optical performance comes a corresponding need for improved definition and quantification of the distortion of an optical window. Distortion can be subjectively determined by a viewer looking through the window [1], but this is difficult to quantify and is not repeatable. Consequently, a wide range of window distortion measurement approaches have been proposed [1,2]. Some apply only to windows with large distortions that can be determined by measuring surface variations [3] and some require specialized components, such as an array of microlenses [4]. By far, the most common method for measuring distortion is to compare images that were photographed with and without the window [1,5-7], but this approach has limited resolution and is not applicable to higher-quality windows. A newer approach, based on moiré interferometry [8,9], has higher resolution, but yields imagery that can be difficult to quantify. In this paper, we propose a new method for quantifying distortion based on phase-shifting interferometry.

## 2 DISTORTION DEFINITIONS

The window attribute that causes image distortion is curvature, whether introduced through a variation in the window thickness or by a localized variation in the index of refraction of the window. It is assumed that these curvatures are very gradual relative to the wavelength of light and that the window surfaces are very smooth, i.e., polished. This is important. Window variations on the order of wavelengths will scatter light and cause image aberrations such as light streaks and diffracted images. These are not attributes of distortion and are ignored in the present discussion. So it is assumed that all window imperfections are very large compared to an optical wavelength and smoothly varying.

Figure 1 shows an idealization of a section of a window. One side of the window is assumed to be perfectly flat while the other side is slightly curved with a radius of curvature  $R$  that is very large compared to size of this window segment, i.e.,  $R \gg 2a$ . Also, assume that the window has a uniform index of refraction  $n$ . Using a set of coordinate axes on the segment as shown, the curved surface can be expressed by the equation

$$z[x] = p - x^2 / (2R) \tag{1}$$

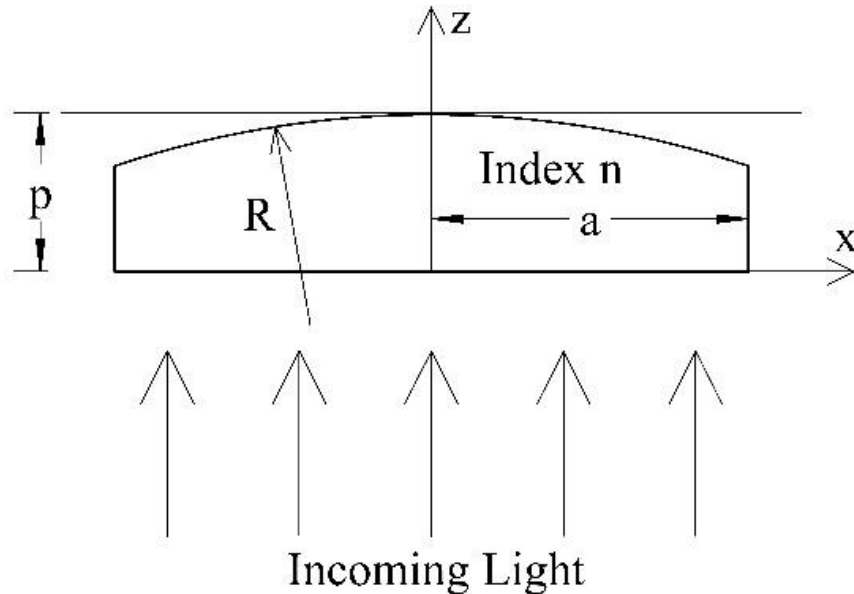


Figure 1. Window Segment with Distortion. This sketch shows a small section of a window with one planar surface and one constant curvature surface and is used as a model of a small section of a window having distortion.

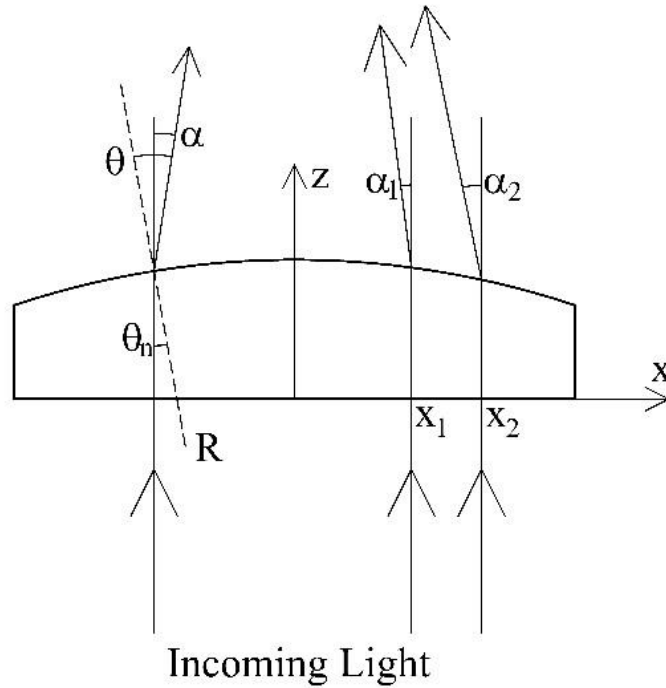


Figure 2. Light Refraction by a Window Segment. This sketch shows how rays of light are refracted by the curved surface representing a small segment of a window.

### 2.1 Distortion Definition 1

The most common definition of distortion is based on tracking rays of light that pass through the mirror. Referring to Figure 2, a beam of light that passes through the window at location  $x_1$  is deflected by an angle  $\alpha_1$ , while a parallel beam, a short distance away at location  $x_2$ , is deflected by an angle  $\alpha_2$ . This change in the deflection of light versus position leads to the first definition of distortion  $D$ , namely

$$D \equiv \frac{\alpha_2 - \alpha_1}{x_2 - x_1} \quad (2)$$

If the surface curvature is gradual and the sampling distances small, this expression becomes the derivative of the angular deviation with respect to location, i.e.,

$$D \equiv \frac{d\alpha[x]}{dx} \quad (3)$$

This definition is used by the military in specifying distortion; for example, an optical flat should have less than 1 minute of arc per inch distortion [1] and is the basis of the ISO standard [6]. It suggests several ways to measure distortion, including looking through small regions of the window with a telescope and launching laser beams through the window.

Using Snell's law, we can relate this definition to the surface curvature and the index of refraction of the window. In Figure 2, an incoming ray of light hits the curved surface at an angle  $\theta_n$  to the normal, shown by the dashed line that leads back to the center of the radius of the curvature  $R$ . This ray of light is refracted by an angle  $\theta$  towards the  $z$  axis. The goal is to find the deviation angle  $\alpha$  as a function of  $x$ , so its derivative can be calculated. Start with Snell's law  $n\sin[\theta_n] = \sin[\theta]$ , which, since the curvatures are all very gradual, can be converted into a small angle form, i.e.,  $n\theta_n = \theta$ . Now, note that the slope of the window's curved surface is equal to  $\theta_n$  and that this slope is also equal to the derivative of Eq. (1). Finally, looking at the figure, it is seen that  $\alpha = \theta - \theta_n$ . Combining these yields

$$\alpha[x] = \theta - \theta_n = (n-1)\theta_n = (n-1)\frac{d}{dx}\left(p - x^2 / (2R)\right) = -\frac{(n-1)}{R}x \quad (4)$$

So from Eq. (3) the distortion is found to be

$$D = \frac{d\alpha[x]}{dx} = -\frac{(n-1)}{R} \quad (5)$$

This agrees with our initial requirement that a planar surface, i.e., one with infinite radius of curvature, has zero distortion. It also indicates that as the curvature becomes smaller, the distortion becomes larger—a reasonable result.

## 2.2 Distortion Definition 2

A second definition of distortion is given by the American Society for Testing and Materials (ASTM) [5] and states that distortion is equal to one over the focal length  $F$  of the lens formed by the curvature of the window, i.e.,

$$D \equiv (1/F) \quad (6)$$

This definition describes distortion in terms of local curvature, resulting in local focusing, or defocusing, of light passing through the window. In order to find the focal length of the lens formed by the curved window surface in Figure 1, we need to ask where on the  $z$  axis do the refracted rays converge. Using a small angle approximation, we see that  $\alpha[x] \approx x/F$ . Using this result and Eq. (4), the second definition of distortion yields

$$D = (1/F) = \alpha[x]/x = -(n-1)/R \quad (7)$$

As expected, these two definitions yield the same result, though they start with very different physical intuition.

### 2.3 Distortion Definition 3

The third definition of distortion—presented for the first time in this paper—is based on a fundamental window attribute, namely the window’s optical path length function,  $\sigma[x]$ . This function describes the distance, as seen by the light, as it travels through the window and the air, from one plane to a second plane. So calculate the optical path length in Figure 1 as light moves from the lower planar window surface at  $z = 0$  to the  $z = p$  plane. For each value of  $x$ , the light passes through an amount of glass given by  $z[x]$  in Eq. (1) and then passes through an amount of air given by  $p - z[x]$ . So the optical path length function is given by

$$\sigma[x] = n(z[x]) + (p - z[x]) = (n-1)(p - x^2 / (2R)) + p \quad (8)$$

The derivative of this function describes the direction that the light takes after passing through the window and air, i.e.,

$$d\sigma[x] / dx = -(n-1)x / R = \alpha[x] \quad (9)$$

The second derivative of this function provides the third definition of window distortion

$$D \equiv \frac{d^2\sigma[x]}{dx^2} = -\frac{(n-1)}{R} = \frac{d\alpha[x]}{dx} \quad (10)$$

showing that the distortion of a window can be expressed as the second derivative of the optical path length function. This is important because equipment now exists, namely phase-shifting interferometers, which can easily and quickly provide the optical path length function of a window accurately and with high resolution.

### 2.4 Component and Total Distortion

Real-world windows extend in two dimensions, although the definitions given above for distortion are only one-dimensional. The ASTM resolves this by defining three different distortions,  $D_x$ ,  $D_y$ , and  $D$  [5]. The  $D_x$  and  $D_y$  distortions are defined in terms of the angular deviation of light when scanning the window in the  $x$  and  $y$  directions, but no relation between these component distortions and the distortion  $D$  is provided. The ISO standard states that optical distortion on a window is equal to the maximum distortion found by measuring in all directions [6]. This is better than the ASTM method, but is still unclear because distortion can change sign.

Our new definition of distortion removes this confusion by the following straightforward extensions of the one-dimensional definition given above in Eq. (10):

$$D_x \equiv \frac{d^2\sigma[x, y]}{dx^2} = \frac{d\alpha[x, y]}{dx}, \quad D_y \equiv \frac{d^2\sigma[x, y]}{dy^2} = \frac{d\alpha[x, y]}{dy}, \quad D = D_x + D_y = \nabla^2\sigma[x, y] \quad (11)$$

This states that the total distortion  $D$  is the sum of the two component distortions and is represented by the Laplacian of the optical path length. This definition is mathematically consistent with the intuition that the distortion should be related to the window curvature, but it should be stressed that window pass-fail criteria must be carefully written. For example, if the window is saddle-shaped,  $\sigma[x, y] \propto xy$ , then  $D_x$ ,  $D_y$ , and  $D$  in Eq. (11) are all zero, yet the window is not flat.

### 3 THE IMAGE COMPARISON METHOD

Having the various equivalent definitions of distortion, we can now compare three different methods for measuring distortion. We will start with a straightforward technique where a test pattern is photographed at some distance with and without the window and the two images compared. Then a newer technique using moiré interferometry will be tried. The third approach will use a phase-shifting interferometer. In all three cases, we will examine the same window, a roughly 6-inch-diameter section of acrylic sheet (3/16 inch thick) that has appreciable distortion. This is of interest because future spacecraft are being designed with plastic windows instead of fused silica in order to save weight, even though plastics typically have greater window distortion than the fused silica windows they are replacing.

A distortion measurement system was constructed as described in the ASTM standard [5] and is shown in Figure 3. An image of a set of parallel dark lines spaced apart by 1 cm was created. This image was located 3.6 m (distance  $2L$  in Figure 3) from a focusing lens with focal length  $f$ . After this reference image was photographed, the acrylic window was placed between the image and the lens and a second photo was taken. The acrylic window was then rotated by 90 degrees and a third photo taken. The presence of the acrylic window causes the photographed lines to be shifted and deformed. By measuring the amount of shift in the line segments, we can calculate the distortion in the corresponding section of the window.

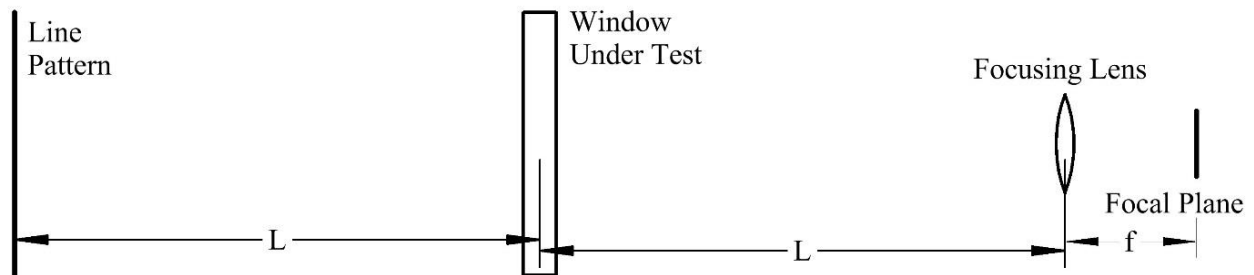


Figure 3. Image Comparison Optical System. This is a sketch of the distortion measurement system using image comparison.

#### 3.1 Mathematical Analysis

Repeating the system parameters, the line pattern consists of parallel black lines on a white background, spaced apart by 1 cm. This line pattern is placed a distance  $2L$  from a focusing lens ( $L = 1.8$  meters). The lens (74 mm focal length) focuses the pattern onto a camera's focal plane array. The pixel spacing on the focal plane is 4.65 microns, and the array is 1040 pixels high and 1392 pixels wide.

First consider the system with the window removed as shown in Figure 4. A specific line, a distance  $d$  above the centerline, is focused by the lens onto the focal plane at a distance  $x_1$  below the centerline of the array. Note that the angles are small so that  $\alpha \approx d / (2L) = x_1 / f$ .

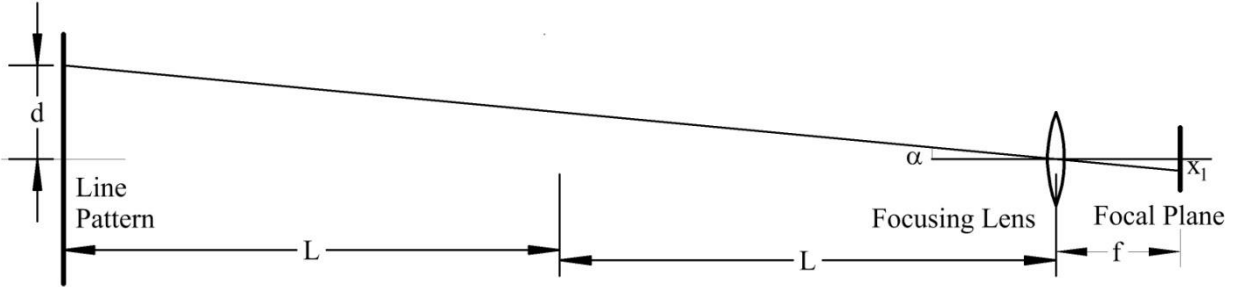


Figure 4. Image Comparison Math 1. This sketch shows a ray of light coming from the line pattern and being imaged onto the focal plane array without the window present.

Now put the window halfway between the lens and the line pattern as shown in Figure 5. The window causes the rays of light to be deflected from an incoming angle  $\alpha_2$  to an outgoing angle  $\alpha_3$ . We want to find the deflection angle  $\alpha(x, y) = \alpha_2 - \alpha_3$  over the window. The line image that was focused onto the focal plane array at location  $x_1$  is now focused onto the focal plane array at location  $x_2$ . We can measure the shift  $\Delta x = x_1 - x_2$ , so we need to find an equation to convert this measurable image shift to a deflection angle.

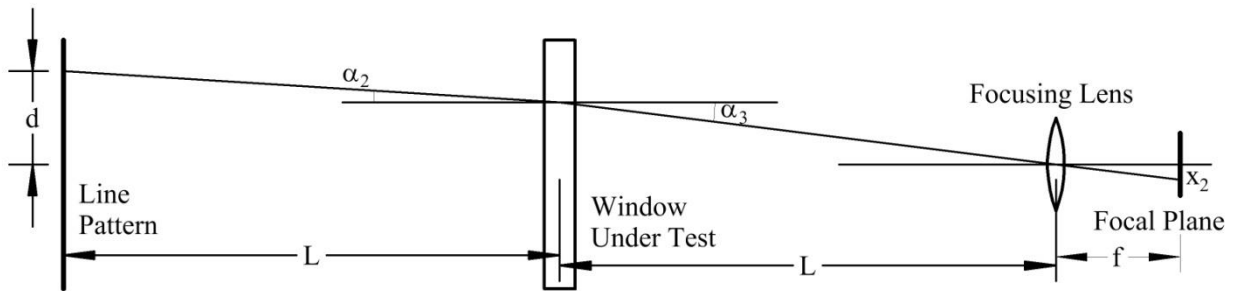


Figure 5. Image Comparison Math 2. This sketch shows a ray of light coming from the line pattern and being imaged onto the focal plane array with the window present.

In Figure 5, the distance  $d$  is now given by

$$d = \alpha_2 L + \alpha_3 L \tag{12}$$

and since  $d = \alpha 2L$  we find that

$$\alpha = \frac{\alpha_2 + \alpha_3}{2} . \quad (13)$$

In other words, the angle without the window is the average of the angles with the window. Now, note that

$$x_2 = f \alpha_3 \quad (14)$$

so we can write

$$\Delta x = x_1 - x_2 = f(\alpha - \alpha_3) = f\left(\frac{\alpha_2 + \alpha_3}{2} - \alpha_3\right) = f \Delta \alpha / 2 . \quad (15)$$

So the angular deviation is

$$\Delta \alpha = 2(x_1 - x_2) / f . \quad (16)$$

Using Eq. (16), if we can develop an algorithm to find the change in the focal spot on the focal plane array, we can then find the angular deviation of the window.

### 3.2 Algorithmic Analysis

The camera images were saved as bitmaps and imported into Mathematica, where custom software was written to process the images. Figure 6 shows the cropped line pattern images without the window (left) and with the window (right). The goal is to develop an algorithm that can turn these two images into a mapping of the line offset distance and then use Eq. (16) to find the window deviation map. This was accomplished by plotting the black-and-white pixel intensities in the vertical direction for each horizontal pixel column. A typical plot is shown in Figure 7. Mathematica then found the local minimums of this plot and recorded that as the line location. This process was performed on both images, without and with the window, and the differences found.

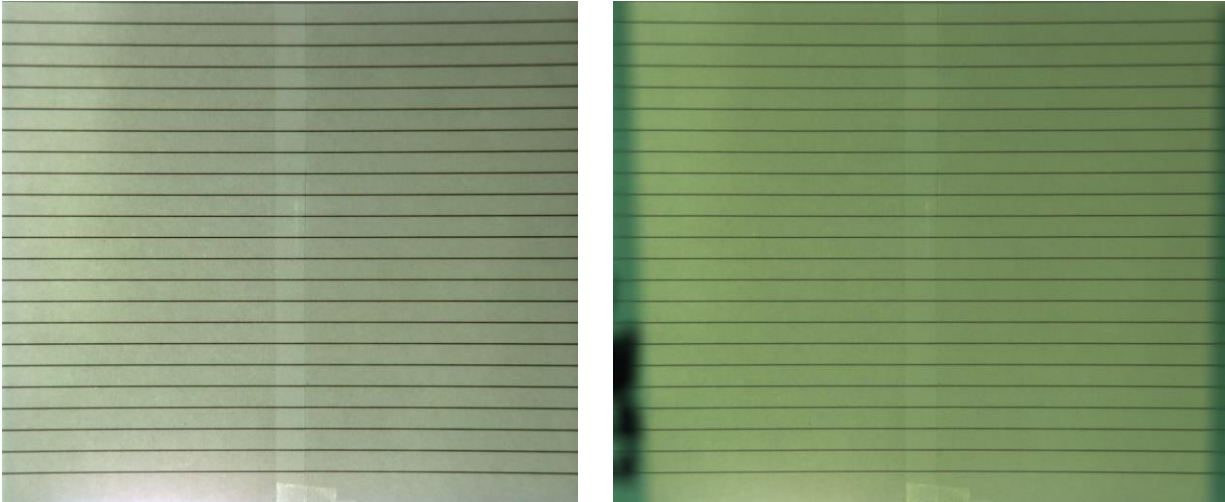


Figure 6. The Line Pattern Images. This figure shows the line pattern images without the window (left) and with the window (right).

Because the vertical resolution is limited to the line spacing, which is 0.5 cm (recall that the line spacing is 1 cm), and the window is halfway between the line pattern and the lens (the window is being measured every 0.5 cm), the horizontal resolution was set to 0.5 cm. This corresponds to about 47 pixels, so the horizontal data was grouped into 47 pixel sets and averaged. We hoped that this would improve the resolution of the measurement to something better than 1 pixel. Using this pixel offset data with Eq. (16) yielded the angular deviation of the window, which is shown in the next section.

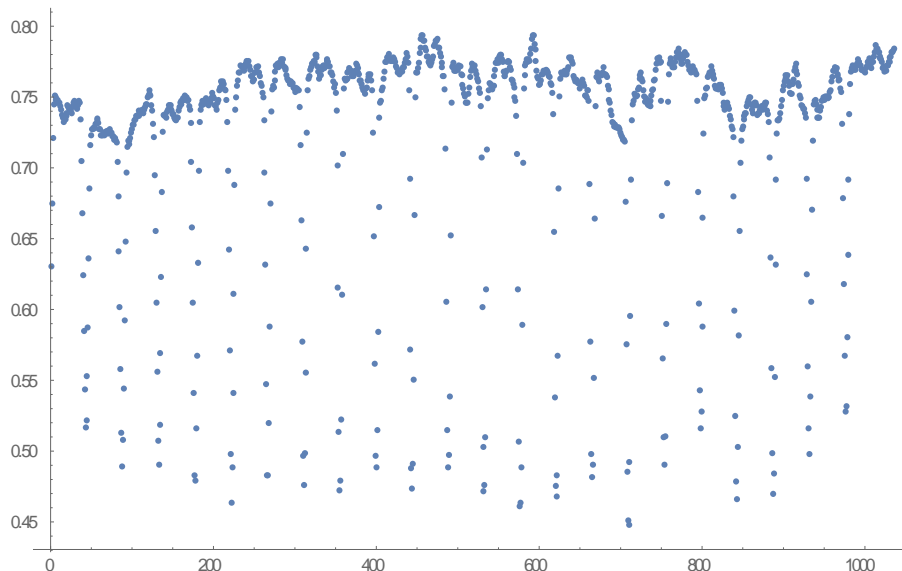


Figure 7. Line Pattern Processing. This is a plot of the vertical black-and-white pixel intensity for an arbitrary horizontal location in the image shown in Figure 6 (left).

### 3.3 Results

Figures 8 and 9 show the angular deviation plots for the acrylic window tested by the image comparison method. The data set provides a value for every 0.5 cm in the horizontal and vertical directions. Mathematica has plotted the data as a surface contour, which provides some smoothing of the result. The absolute values in  $x$  and  $y$  have an arbitrary offset since we did not impose a coordinate system on the window, so the data set simply begins at  $(0, 0)$ .

A one-pixel shift on the camera's focal plane array corresponds to 0.4 minutes of arc. The averaging process may slightly improve this, but the data indicates that this is probably not the case. Figure 9 has a full range of only 0.4 minutes of arc and the data appears to jump back and forth by about 0.4 minutes of arc, indicating the software was stepping by about one pixel. So the resolution of this process is only about 0.4 minutes.

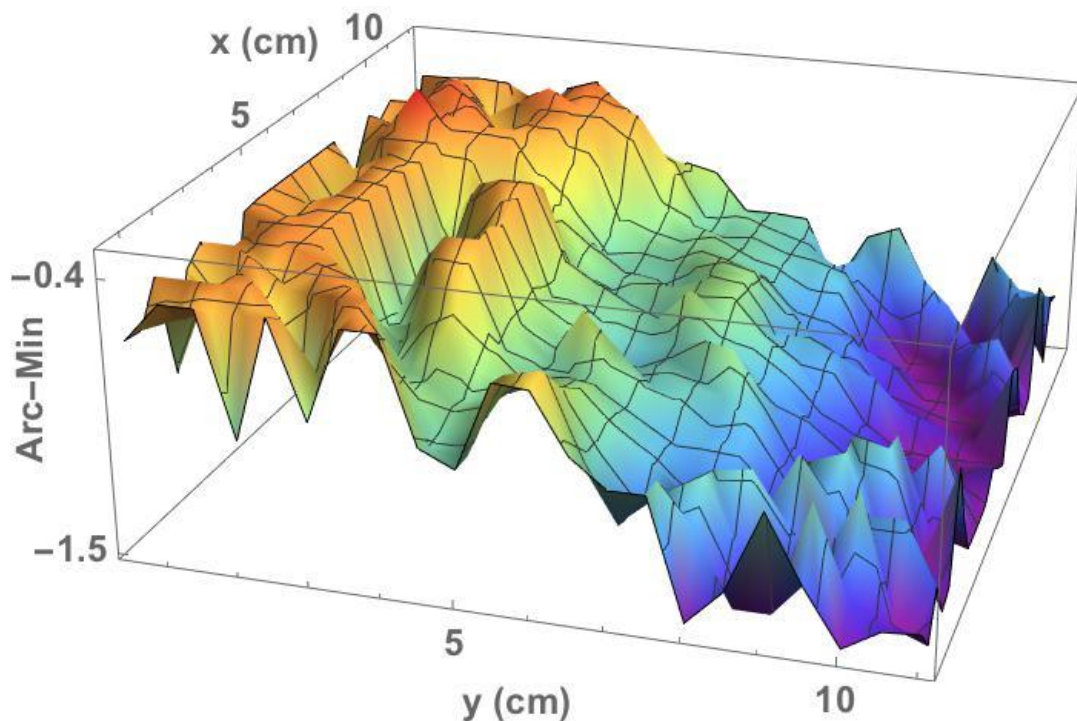


Figure 8.  $y$ -direction Angular Deviation. Measured angular deviations for the  $y$ -direction seen in the acrylic window as a function of location on the window.

Owing to limited resolution, it's difficult to determine the distortion of the window. Taking the derivative of these two plots, as shown in Eq. (1), amplifies the oscillatory nature and swamps what might be true distortion. For example, Figure 8 shows a definite slope across the window corresponding to a large-scale, though small,  $y$ -directed distortion across the window, which is many times smaller than the noise-induced slopes seen in smaller regions.

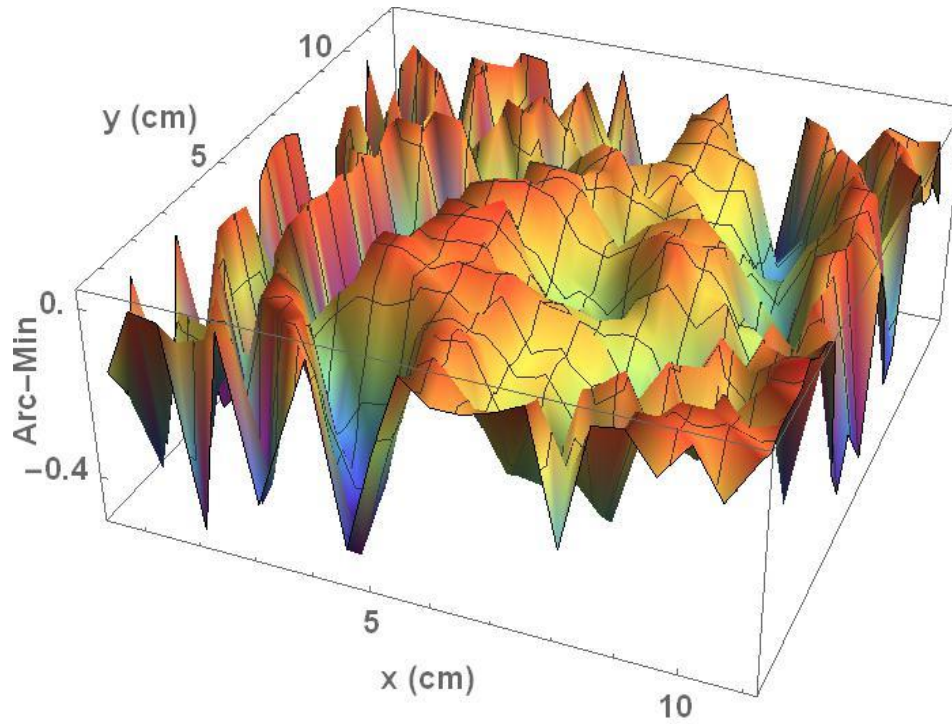


Figure 9. *x*-direction Angular Deviation. Measured angular deviations for the *x*-direction seen in the acrylic window as a function of location on the window.

The image comparison technique is the ASTM standard approach and an approach recommended by the military, but it does not have the resolution to measure the distortion in medium- to high-quality windows. The other two approaches will be shown to offer significant improvements.

#### 4 THE MOIRÉ INTERFEROMETRY METHOD

Moiré interferometry [8,9], like Schlieren imagery [10], is an optical technique that amplifies the intensity variations caused by small angular deviations of light rays. There are several ways to set up a moiré interferometer, and our system choice is shown in Figure 10. Light passes through a transparent lined pattern (i.e., a Ronchi ruling) and travels to a spherical mirror with radius  $R$  (48 inches in our system). The light reflects back and passes through the transparent line pattern a second time, and is imaged onto a camera focal plane. If no window is present, then the light will reflect off the spherical mirror at about the radial line, i.e.,  $\tau_1 = \tau$ , but if a window is present, then the light angle will deviate from this ideal.

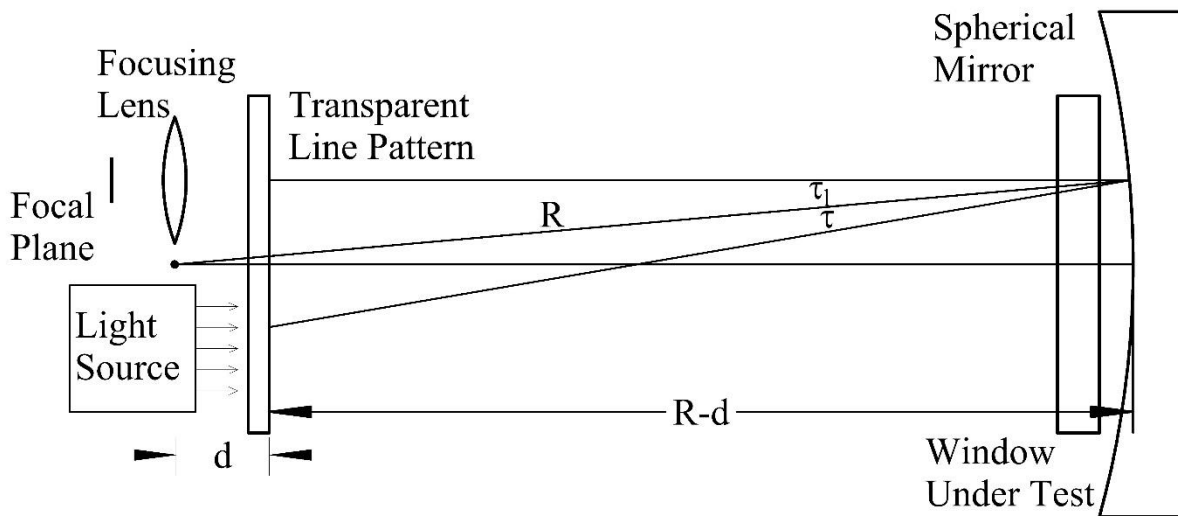


Figure 10. Moiré System 1. A sketch of the moiré interferometry system for measuring distortion.

Figure 11 is a photograph of the system. The setup is relatively simple and the alignment of the optical components is not stringent. Some readers might guess that this is a Schlieren system, and that is correct, except for one critical difference. In a standard Schlieren system, the Ronchi ruling, or transparent lined pattern, is located at the radius of the mirror so that the camera sees a single large “fringe.” In the present system, the Ronchi ruling has been moved closer to the mirror by a distance  $d$ . This causes the camera to see a set of parallel lines and dark lines as shown in the left edge of the mirror in Figure 12. Placing the acrylic window into the system then causes a much more significant shifting of the line pattern than was seen in the direct image comparison approach. So, the goal is to measure the shifts of this light/dark line pattern and convert them back to the angular deviations caused by the window.

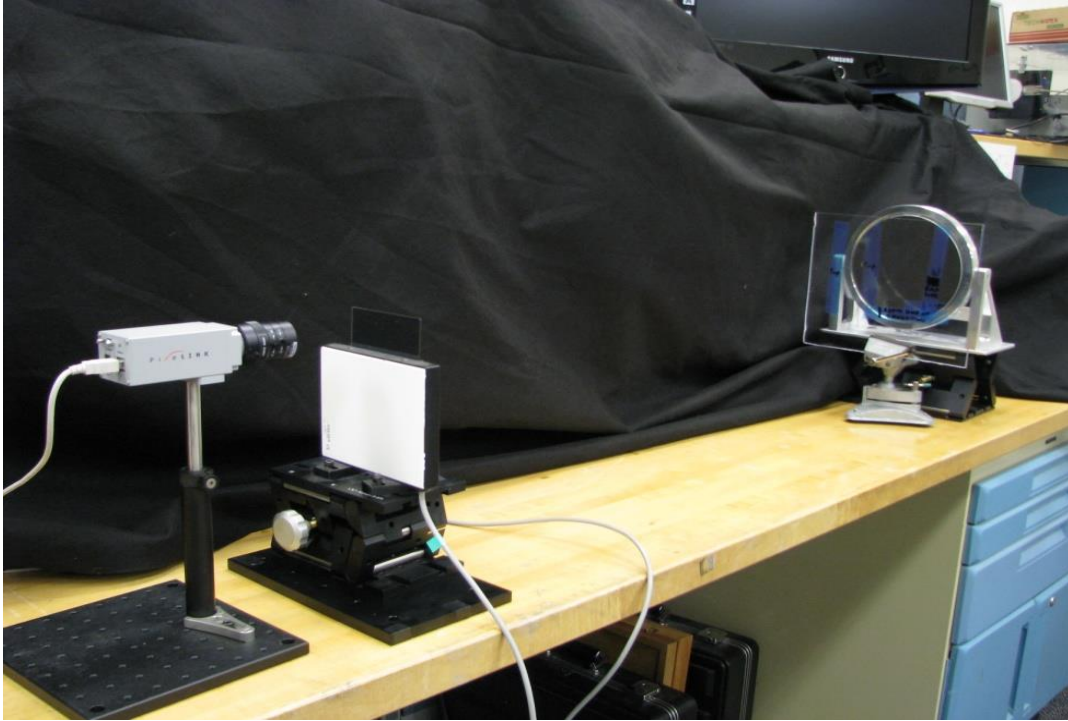


Figure 11. Moiré System 2. A photo of the moiré interferometry system for measuring distortion.

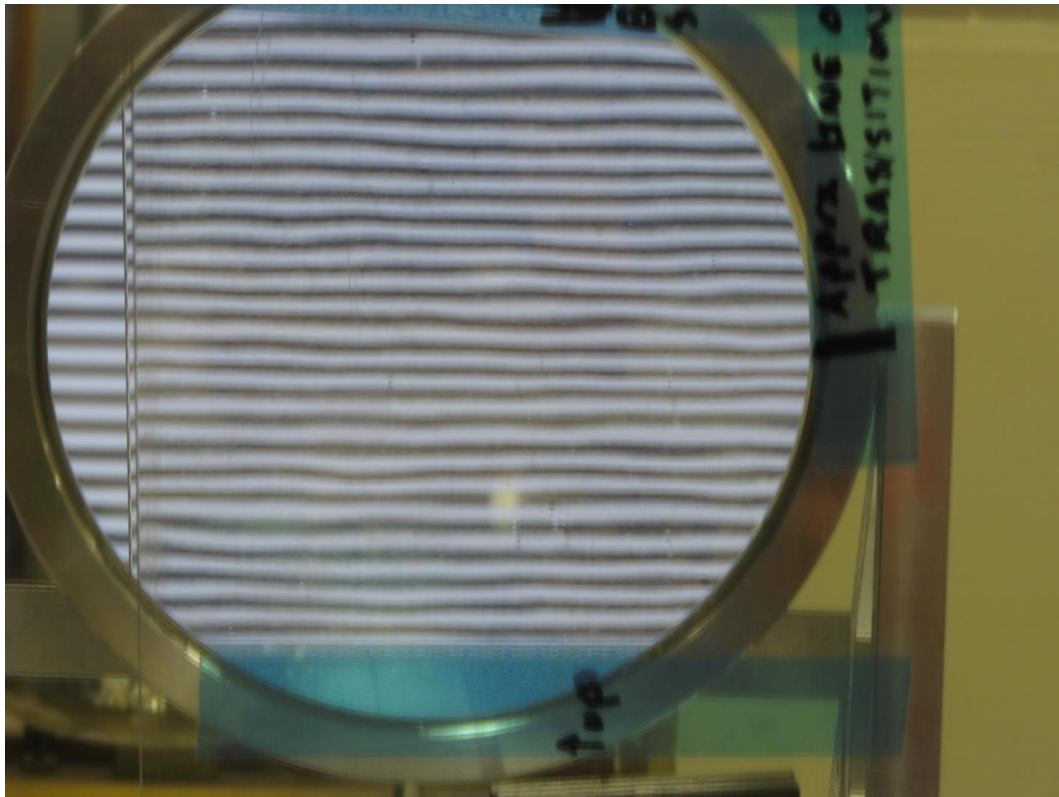


Figure 12. Moiré System Line Deflection. This photo shows the effect of placing a window into the moiré system.

### 4.1 Mathematical Analysis

Let us begin by analyzing the system without a window present. A transparent line pattern, i.e., a Ronchi ruling, is placed such that light will pass through it twice. A light source sends light through the lower side of this element toward a mirror that reflects the light back onto its upper side. The Ronchi ruling is 4 inches square and has 50 parallel black lines per inch, each line being 1/100 inch wide with a 1/100-inch transparent gap. The ruling is placed with the lines horizontal.

A camera with a focal plane array and lens is used to look through the upper half of the Ronchi ruling at the mirror. The mirror is 8 inches in diameter and is spherical with a radius of curvature of 48 inches. Light that hits the mirror along a radial line reflects directly back and light that hits a point on the mirror at some angle off normal,  $\tau$ , will reflect off the mirror, and return on the other side of the mirror normal at angle  $\tau$  as shown in Figure 13.

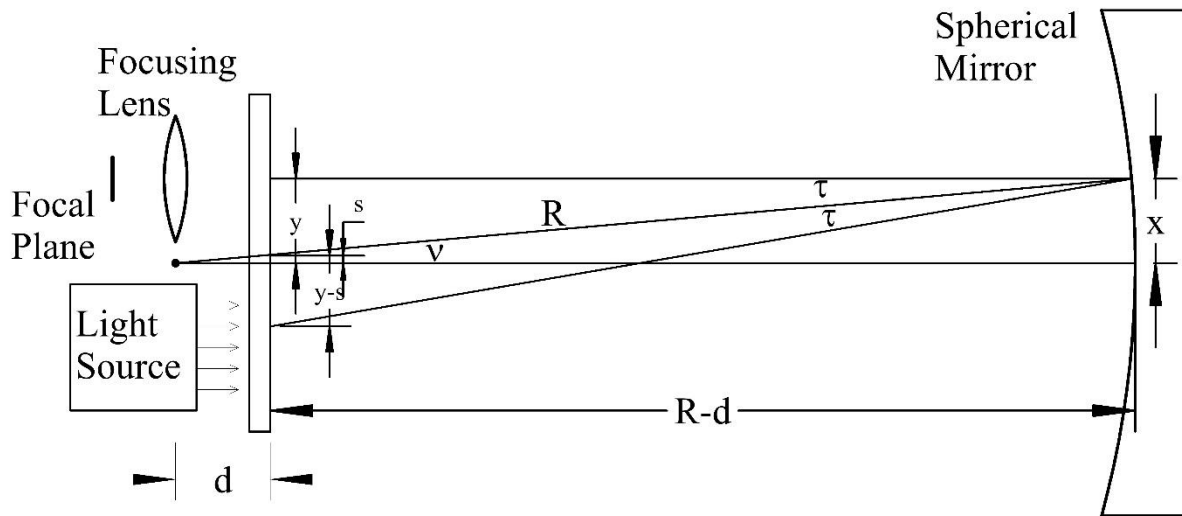


Figure 13. Moiré Math Without Window. This sketch defines some of the system parameters so that analysis without a window present can be performed.

The Ronchi ruling is located a distance  $d$  closer to the mirror than the radius point of the mirror. If the Ronchi ruling were at the radius point, then the mirror would image the ruling onto itself and the field of view could be made uniformly dark or light by translating the ruling up or down (standard Schlieren system). By placing the Ronchi ruling closer to the window, we create moiré lines, as will be shown next.

The camera can only see the light from the light source because it is looking into the mirror, so we can follow our observation line out to the mirror, reflect off the mirror, and see where we end up on the Ronchi ruling. The camera has to look through a gap in the Ronchi ruling to see

anything, so if this gap ends up lined up with a dark line in the lower half of the ruling, the camera will see a dark bar. If it is lined up with a transparent gap, then the camera will see a bright bar.

Let's trace a light ray from the lower half of the Ronchi ruling to a point  $x$  on the mirror and then to a point  $y$  above the centerline of the ruling. As we can see in the figure, our light ray hits the mirror at some angle  $\tau$  from normal, so it reflects at an angle  $\tau$  towards the camera. Because the Ronchi ruling is moved forward a distance  $d$ , the radial line from the mirror passes through the Ronchi ruling a distance  $s$  above the centerline. By symmetry, the light ray that hits the Ronchi ruling a distance  $y-s$  above the radial line has to emerge a distance  $y-s$  below this radial line. So the distance on the Ronchi ruling between where the light started and where it ended is equal to  $2(y-s)$ .

Now, the small angle formed by the radial line with the horizontal can be expressed as  $v = x/R = s/d$ , so  $s = xd/R$ . Using this result, we find that the distance between input and output on the Ronchi ruling is  $2(y - xd/R)$ , where the important result is that this spacing is a function of  $x$ . In other words, as the camera looks at different heights on the mirror, it is seeing different source locations on the Ronchi ruling. As the Ronchi ruling is scanned, the result is the appearance of a series of parallel horizontal dark and light bars. The spacing between two dark bars,  $w$ , corresponds to the Ronchi ruling spacing ( $f = 1/50$  inch), algebraically  $f = 2wd/R$ . In our case  $R = 48$  inches and  $d = 2.5$  inches, so the dark bar spacing should be about  $1/5$  inch, which is what we observe.

Let's ask a question. How much would we have to tilt the mirror to move the dark bar pattern up or down one bar? If we tilted the mirror by a very small angle  $u$ , the point  $s$  would move a distance  $u(R-d)$ , so the distance between the Ronchi ruling in and out points would change by twice this,  $2u(R-d)$ . This must equal one Ronchi ruling spacing to move one dark bar, i.e.,  $1/50$  inch. So,  $u = f/(2(R-d)) = 0.00022$  radians or in other units,  $0.0126$  degrees, which is also  $0.76$  minutes of arc. Another way to say this is that if a returning beam of light that would be blocked by the ruling is tilted down by  $1.5$  minutes of arc, then it will hit the Ronchi ruling  $1/50$  of an inch below its previous location and will hit another dark line on the ruling.

Now, let's put a window into the system as shown in Figure 10. The window will deflect light by some small amount,  $\alpha(x, y)$ , which is doubled because the light passes through the window twice. Consequently, the light does not emerge at the same angle as it went in relative to the window,  $\tau_1 = \tau - 2\alpha(x, y)$ . So the line pattern will appear to have been shifted up or down, where one-band spacing corresponds to  $1.5$  minutes of arc, i.e.,  $\alpha(x, y) = 0.75$  min of arc causes one full line shift.

There is an additional problem. Putting in a perfect window causes a line shift, so this effect must be removed from the data. If we had a perfect window, we could use this to calibrate the

system; but since we do not have a perfect acrylic window, we will do this through modeling. Referring to Figure 14, when a ray of light enters the window at some angle  $\theta$ , it is refracted to a new angle  $\theta_n \approx \theta/n$ , passes through the window, and then refracts back on the far side of the window so that it is traveling parallel to the path it would have traveled if the window had not been there, but shifted. So the ray hits the mirror at the same angle that it would have without the window, but at a distance  $h(n-1)\theta$  lower, where  $h$  is the thickness of the window and  $n$  is its index. If we move down the mirror a distance  $h(n-1)\theta$ , this means that we have moved down an angular distance equal to  $h(n-1)\theta/R$ , so the normal angle to the mirror has changed by an angular amount equal to  $h(n-1)\theta/R$ . The ray of light bounces off the mirror about this normal line (shown as dashed lines in Figure 14). So if the window had not been there, it would have reflected back at angle  $\tau$  as seen in Figure 13. Since the ray is shifted down the mirror, the normal has tilted by a small angle and the reflected ray acquires an extra  $2h(n-1)\theta/R$  radians on its direction of travel. In our case, this equals  $2(3/16 \text{ inch})(1.491-1)(x/R)/R$ . So we get 0.00008 rad/inch of additional angular deflection along the window, i.e., 0.28 min/inch = 0.11 min/cm. So over a 6-inch region, we see about 1.65 minutes of arc change, which is about one full band of additional shift. This partially accounts for the extra lines seen in Figure 12 with the window present.

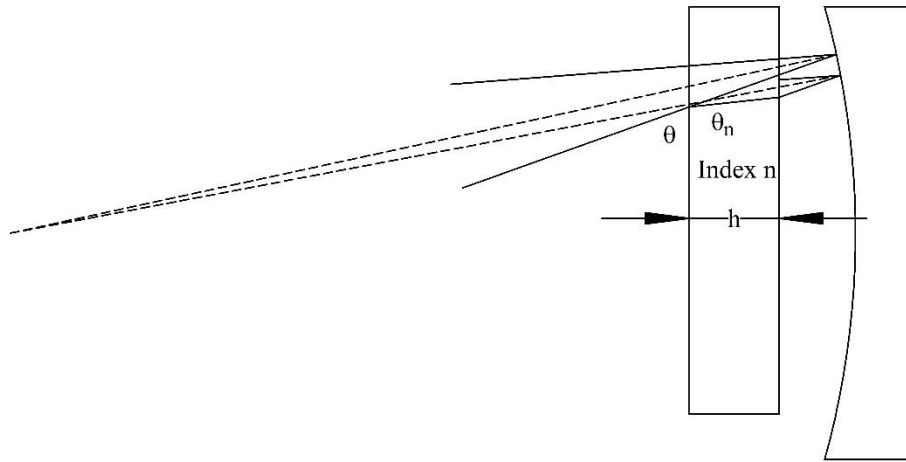


Figure 14. Moiré Math Perfect Window. This exaggerated sketch shows the light ray paths without a window and with a perfect window.

## 4.2 Algorithmic Analysis

Figure 15 shows the moiré pattern produced by the moiré interferometer without and with the window present. The goal of the analysis is to match line segments in the left image with line segments in the right image in order to find the angular deviation caused by the window.

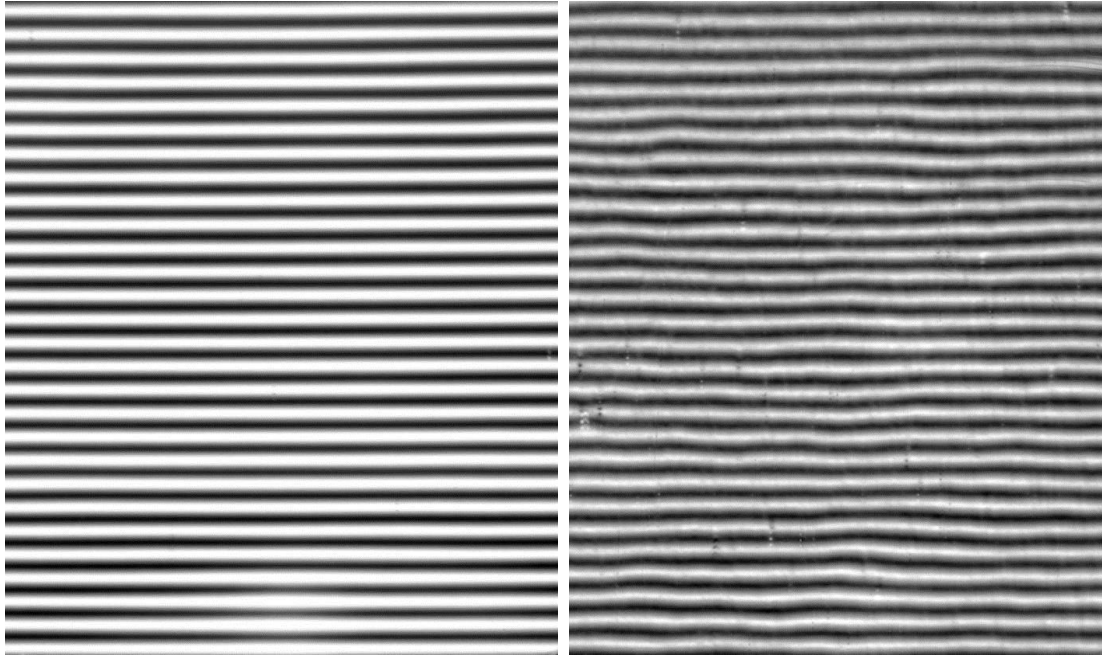


Figure 15. Moiré Pattern Lines. The moiré pattern without and with the window.

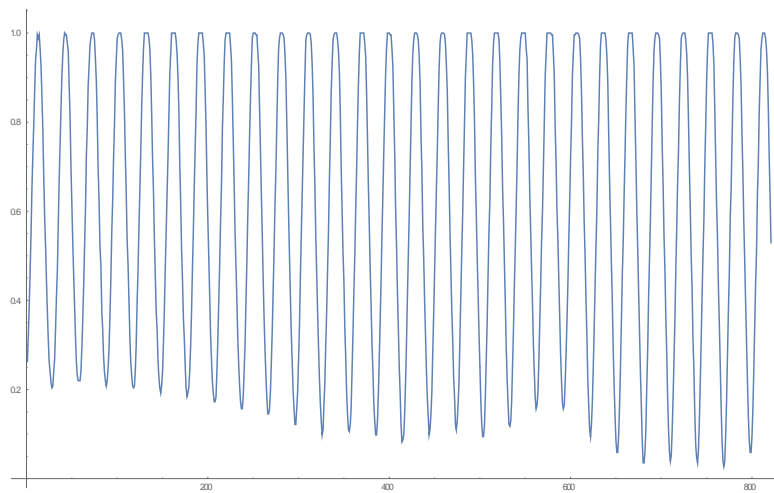


Figure 16. Line Pattern Processing. This is a vertical plot of the light/dark line pattern shown in Figure 15 for an arbitrary horizontal location.

We start the analysis in the same fashion used for the image comparison approach. We acquire the imagery and then plot the intensity profile along a vertical column of the moiré pattern, as shown in Figure 16 and ask Mathematica to locate the local minimums. We do this for both images shown in Figure 15 and then match up line segments to find the total shift of a line. Note that this is somewhat arbitrary because it is not clear what line in the left image corresponds to what line in the right image, but this choice simply adds an offset to the data that will drop out when we take the derivative to find the distortion.

Now recall that one full line shift corresponds to 0.75 minutes of arc, so we can calibrate the imagery. The dark line spacing is about 30 pixels, so the conversion from pixel count to minutes of arc is about 0.75/30; however, before converting we need to subtract off the perfect window angular deviation found in the previous section (see Figure 14). So the formula to convert from line segment shift in pixel count (call this pixel offset) to angular deviation in the window is

$$\left[ (0.28 \text{ min/in})(0.2 \text{ in/line})(\text{line number}) + \frac{1.5 \text{ min/line}}{30 \text{ pixels/line}}(\text{pixel offset}) \right] / 2 \quad (17)$$

The division by two is to compensate for the double pass through the window.

This equation was used for each vertical column, but then 30-pixel segments were averaged to yield one result every  $\frac{1}{2}$  cm. The net result is four measurements for every square centimeter of the window.

### 4.3 Results

The angular deviation plots obtained using the above algorithm are shown in Figures 17 and 18.

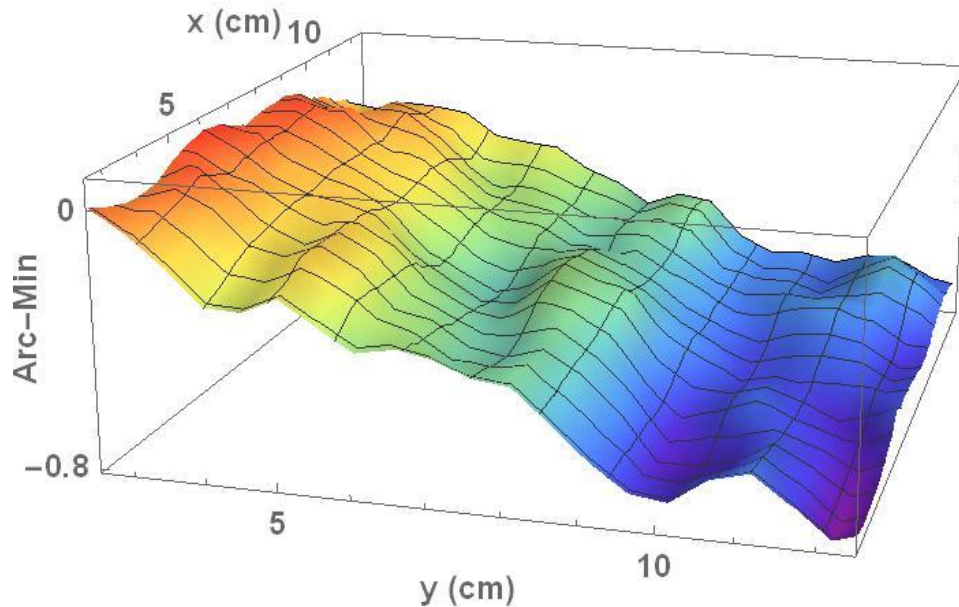


Figure 17. Moiré Angular Deviation in  $y$ . The measured angular deviations seen in the acrylic window as a function of location on the window for the  $y$ -direction.

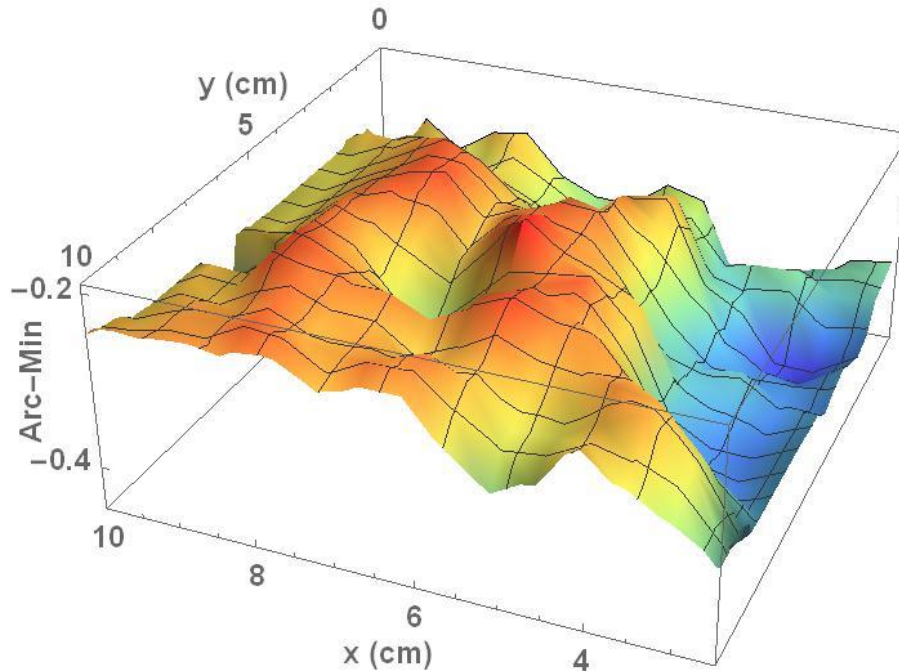


Figure 18. Moiré Angular Deviation in  $x$ . The measured angular deviations seen in the acrylic window as a function of location on the window for the  $x$ -direction.

The data has been plotted, just as before, as contour surfaces using Mathematica. These plots should be compared to the equivalent angular deviations plots using the image comparison approach shown in Figures 8 and 9. As expected, the moiré interferometry approach is more sensitive and has a much smaller pixel error. Assuming the minimums can be found to one pixel resolution, the moiré interferometry approach has  $0.75 \text{ min}/30 \text{ pixels} = 0.025 \text{ minutes of arc error}$ . This is almost 20 times better than the result from the image comparison approach.

The moiré interferometry approach has sensitivity, but accuracy and surface resolution are issues. The light passes through the window twice, but not in exactly the same location since the mirror deflects the light. Also, the analysis shown above has several approximations, none too serious, but care should be taken to ensure that the mirror radius of curvature is significantly larger than the size of the mirror itself so that the multiple small angle approximations made above do not cause a net accumulation of error. If large optics are available, a moiré interferometer can be constructed with a flat mirror and parallel light rays, which will remove much of the complexity of the analysis.

## 5 THE PHASE-SHIFTING INTERFEROMETRY METHOD

Phase-shifting interferometry is a standard technique for measuring the optical path length of optical components. Several companies sell complete systems, typically used for evaluating optical components. For our work, we used a Zygo Corporation Verifire ATZ system [11], as shown in Figure 19, with a 6-inch-diameter measurement capability. References available via the Internet explain how phase-shifting interferometry works, so we will not describe the operation of this system here.



Figure 19. Zygo Phase-Shifting Interferometer. This is a photo of a Zygo phase-shifting interferometer, the Verifire ATZ.

A phase-shifting interferometer measures the difference in optical path length between two reference mirrors. So, before a window is inserted into the system, the optical path length with just the reference windows is measured to provide a background measurement. Figure 20 shows the system output screen when looking at just the reference mirrors. The color plots show the optical path length difference between the mirrors, with any constant offset or tilt removed, leaving only the curvature differences. The reference mirrors are very high quality elements, advertised as having less than 1/10 wavelength (633 nm) surface deviation from flatness. Note that the peak-valley difference between the two is 0.155 waves, less than 100 nm, over a 6-inch-diameter aperture.

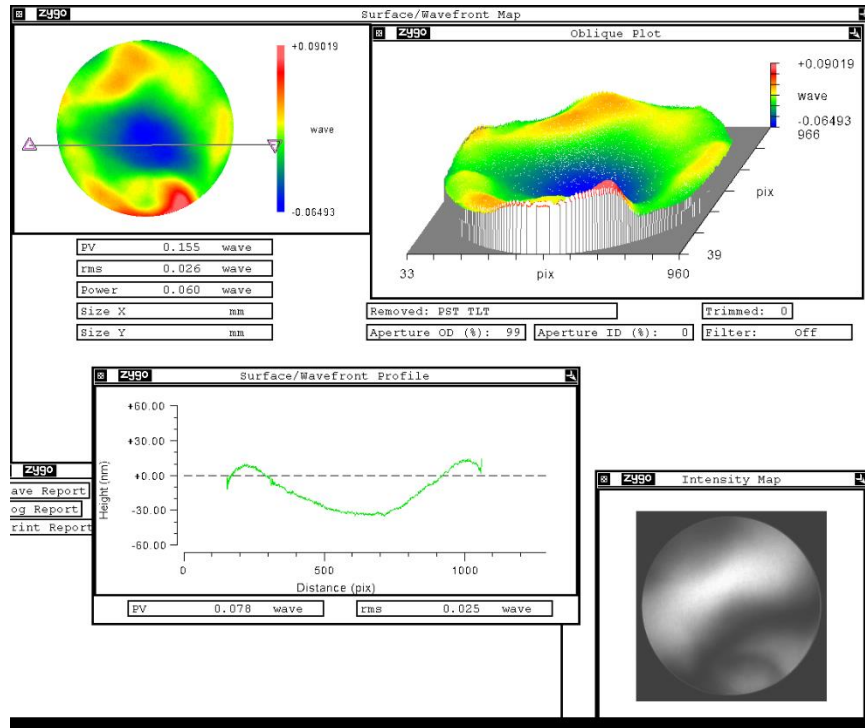


Figure 20. Reference Measurement. This is the output screen from the phase-shifting interferometer when no window is present.

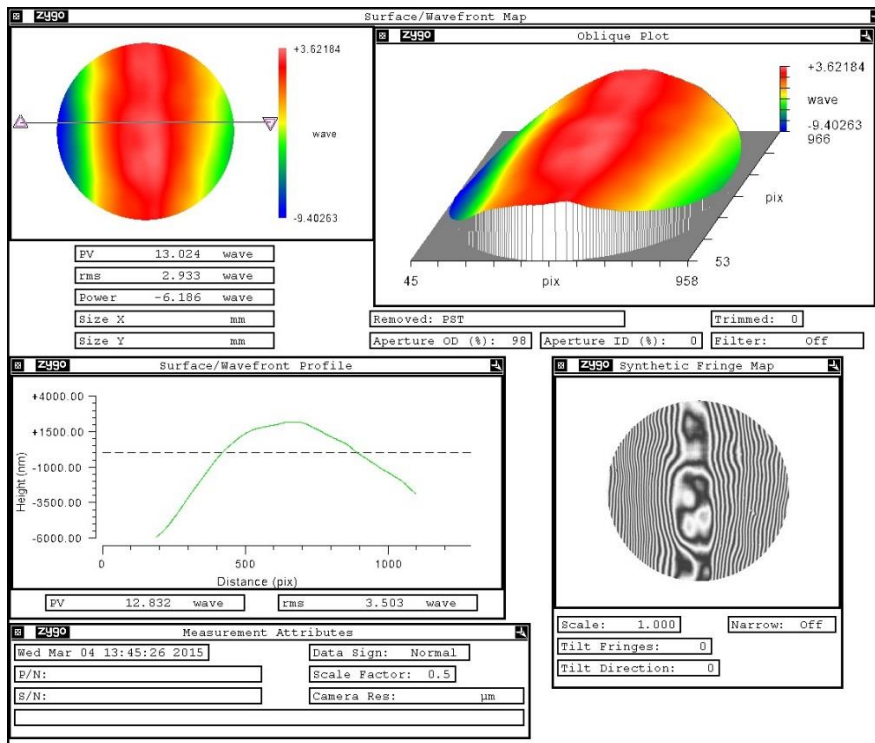


Figure 21. Window Optical Path Length 1. This is the output screen from the phase-shifting interferometer when the window is present.

Inserting the acrylic window yields the optical path length functions shown in Figures 21 and 22. Figure 21 is the output screen from the interferometer and shows the fringe pattern produced by interfering the light received from the two windows, one beam of light having passed twice through the window. The optical path length is shown in both figures where the peak-to-valley difference is now 13 wavelengths (about 8 microns). The Zygo interferometer supplies high-resolution imagery, approximately 60 pixels per cm, and this fine detail is not readily apparent in the screen shots. Using Mathematica, we have cropped out a roughly 11 cm square section of the 6-inch-diameter measurement aperture. This plot is shown in Figure 22, where the fine detail can be seen.

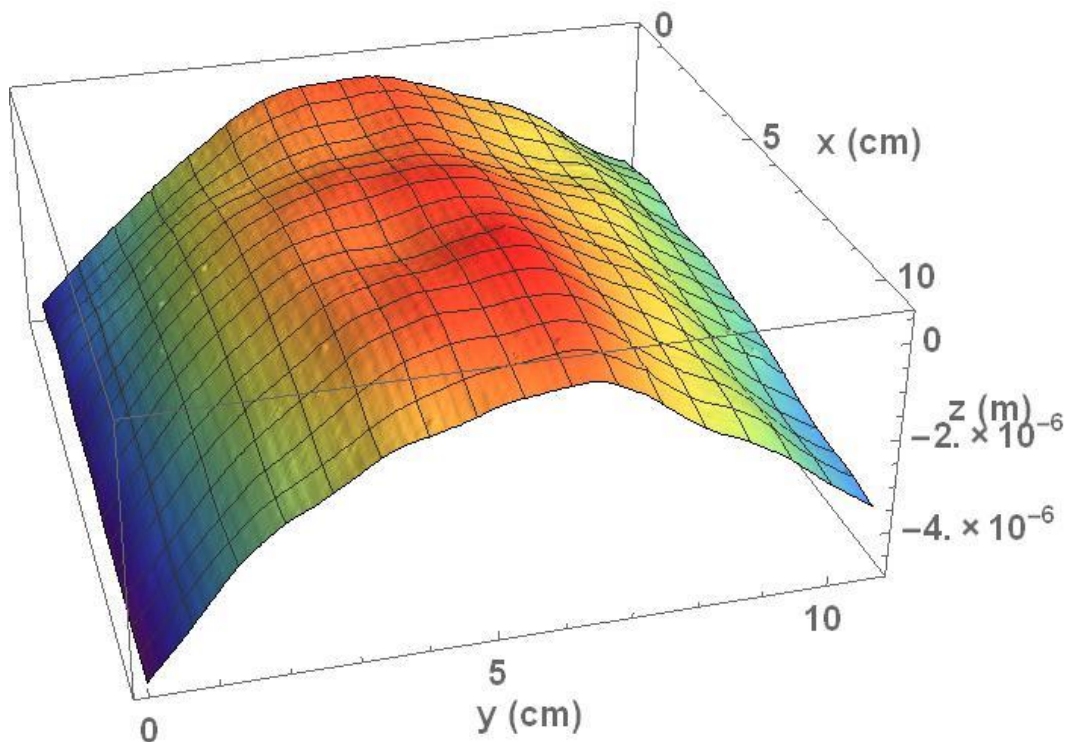


Figure 22. Window Optical Path Length 2. This is a contour plot of the optical path length function of a square section of the window.

## 5.1 Mathematical Analysis

The mathematical analysis is straightforward, as seen in Eq. (11). Simply take the numerical derivative of the optical path length function in each direction to obtain the angular deviation functions and then take derivatives again to obtain the distortion plots.

## 5.2 Algorithmic Analysis

Taking derivatives numerically over very small intervals can cause small signal variations to become large slope changes. To prevent this we have chosen to calculate derivatives by averaging over 1 cm squares and moving the center point in both  $x$  and  $y$  by about 0.083 cm for the angular deviation plots (Figures 23 and 24) and 0.25 cm for the distortion plots.

## 5.3 Results

Figures 23 and 24 show the angular deviation plots in the  $y$  and  $x$  directions for the acrylic window as obtained from taking the derivative of the optical path length function provided by the phase-shifting interferometer. These results should be compared to Figures 17 and 18, as well as to Figures 8 and 9. The phase-shifting interferometer approach yields more accurate data with a much lower noise floor than even the moiré interferometer. However, when comparing these figures, note that we did not attempt to assign an origin to each set of measurements so the  $x$  and  $y$  axes may have an arbitrary offset, and in one case we turned over the window and the resultant plot (Figure 18) is shown with an inverted  $x$ -axis. Also, we did not attempt to determine the offsets in the angular deviation plots. In the previous two approaches, we assigned arbitrary line segments to each other, and in the phase-shifting approach, we adjusted the reference mirror to reduce the fringe count, but at the expense of removing a tilt in the optical path length function corresponding to an offset in the angular deviation plots shown below.

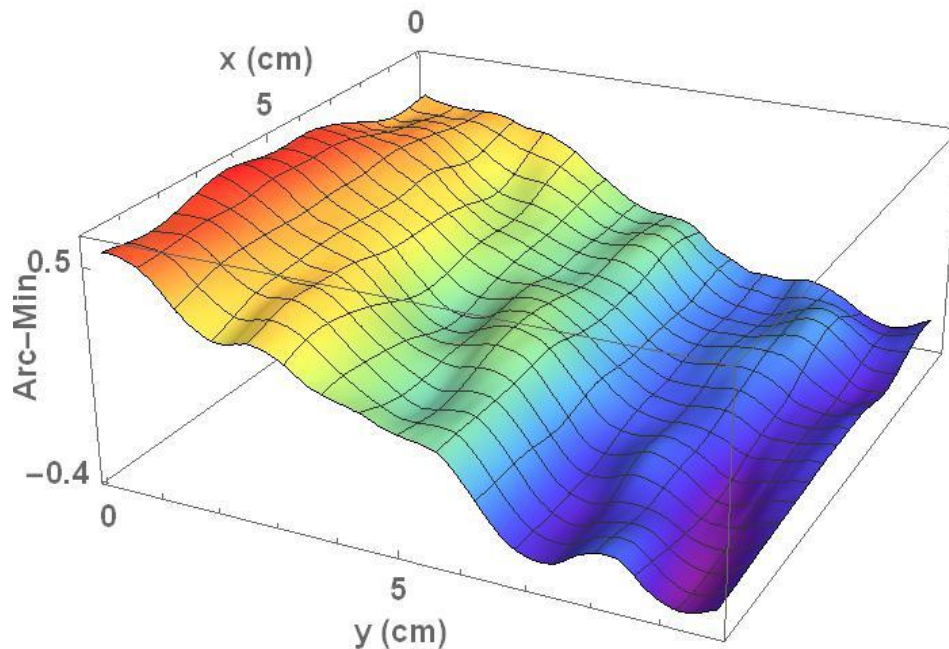


Figure 23. Phase-Shifting Angular Deviation in  $y$ . The angular deviation function in the acrylic window as a function of location for the  $y$ -direction.

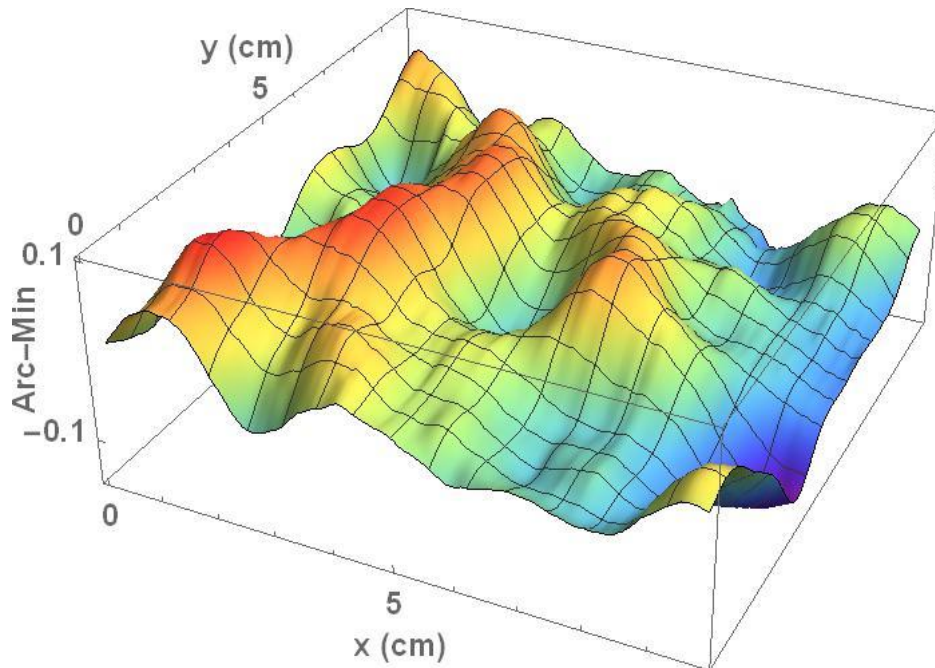


Figure 24. Phase-Shifting Angular Deviation in  $x$ . The angular deviation function in the acrylic window as a function of location for the  $x$ -direction.

The quality of the data from the phase-shifting interferometer is high enough that the second derivatives can be obtained numerically, i.e., the distortion plots shown in Eq. (11). These are shown in Figures 25 and 26. It is interesting to note that the large curvature seen in the optical path length function, which shows up as a slope in Figure 23, has little effect on the distortion plot. It corresponds to roughly a  $-0.1$  min/cm offset in Figure 25, which is difficult to see in the presence of the larger, more localized, distortion effects.

As opposed to the results shown in the image comparison method, the fine structures shown in Figures 25 and 26 are real and are not the result of noise or errors introduced in the derivative process. Phase-shifting interferometers can achieve nanometer optical path length resolution, so distortions much smaller than an arc-second/cm can be measured. For example, consider the reference mirror measurement shown in Figure 20. The line plot shows the optical path length function through a slice of the two-dimensional plot. It has a roughly parabolic shape and corresponds to a curvature, or distortion, of about  $5 \times 10^{-5}$  rad/m = 0.1 arc-seconds/cm, an incredible result.

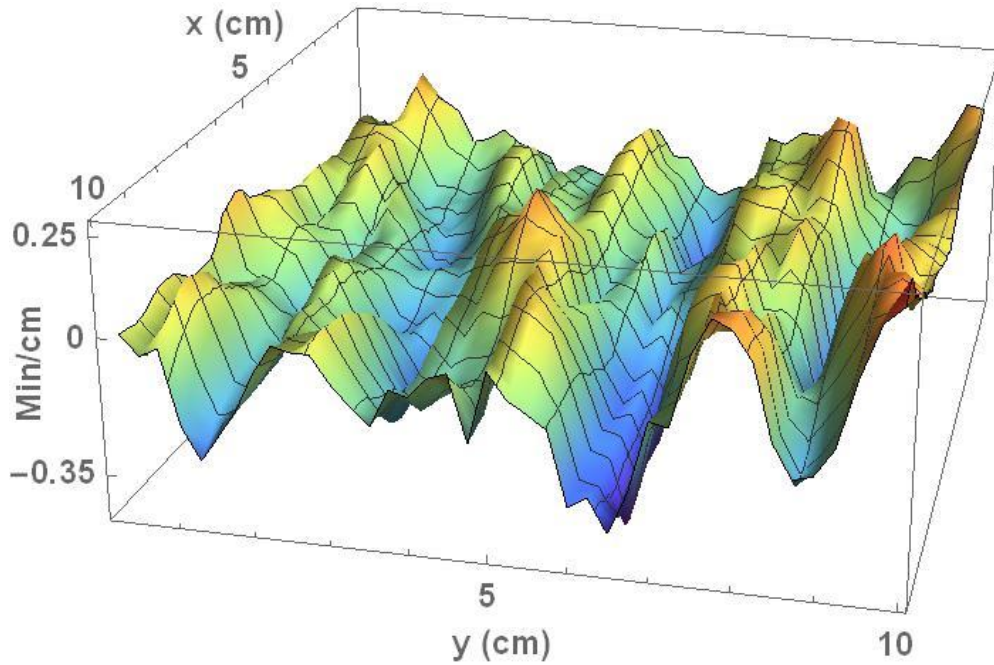


Figure 25. Phase-Shifting Distortion in  $y$ . The distortion function in the acrylic window as a function of location for the  $y$ -direction.

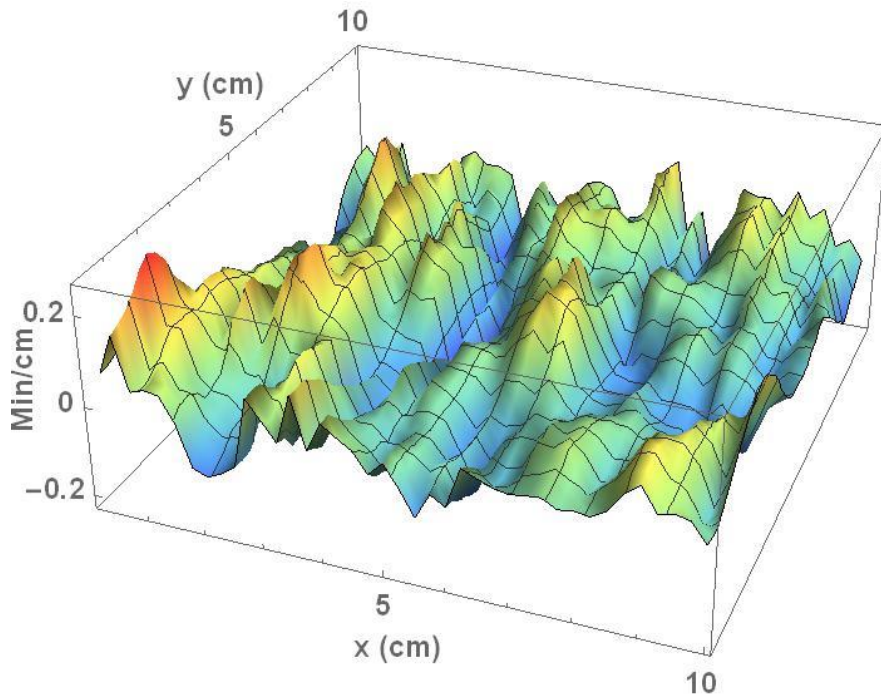


Figure 26. Phase-Shifting Distortion in  $x$ . The distortion function in the acrylic window as a function of location for the  $x$ -direction.

## 6 CONCLUSIONS

We have introduced a new definition of distortion and have shown that it allows a phase-shifting interferometer to be used to determine the distortion of an optical window. At first glance, this technique appears to be preferable over image comparison and moiré interferometry for measuring distortion; however, each method has its strengths and weaknesses. Phase-shifting interferometry provides the highest-resolution measurements, but the system cost is expensive and the dynamic range is limited to only higher quality windows. Also, scanning large-area windows requires making multiple measurements and then stitching the imagery to obtain a complete window map. Moiré interferometry is inexpensive and sensitive, but quantifying the data can be difficult and requires careful measurement and analysis. Even so, once the algorithm is developed, this approach can be scaled to large windows by using a larger spherical mirror and the system sensitivity can be adjusted by changing the spherical mirror's radius of curvature. So it can be used over a wide range of window qualities. Finally, the image comparison approach is the least expensive and most straightforward and has been the standard method for many years. It is adequate when examining poor quality windows, but as shown above, it is limited in performance.

## References

1. J S Harris and K G Harding, ‘Study and Evaluation of Existing Techniques for Measuring Aircraft Windscreen Optical Quality: Development of New Techniques for Measuring Aircraft Windscreen Optical Distortion’, Air Force Aerospace Medical Research Laboratories, Report No. AFAMRL-TR-81-25, February 1981.
2. J S Harris, K G Harding, S H Mersch, ‘Techniques for Evaluation of Aircraft Windscreen Optical Distortion’, *Optical Engineering*, Vol. 20, No. 1, pp. 115-122, January/February 1981.
3. ‘Standard Test Method for Measurement of Roll Wave Optical Distortion in Heat Treated Flat Glass’, American Society for Testing and Materials, ASTM C1651-11, October 2011.
4. M Savolainen, K-E Peiponen, P Savander, R Silvennoinen, and H Vehvilainen. ‘Novel Optical Techniques for Window Glass Inspection’, *Measurement Science and Technology*, Vol. 6, No. 7, pp. 1016-1021, 1995.
5. ‘Standard Test Method for Measuring Optical Distortion in Flat Glass Products Using Digital Photography of Grids’, American Society for Testing and Materials, ASTM C1652M-14, May 2014.
6. ‘Road Vehicles—Safety Glazing Materials—Test Methods for Optical Properties’, International Organization for Standardization, ISO 3538:1997(E).
7. M Dixon, R Glaubius, P Freeman, R Pless, M P Gleason, M M Thomas, W D Smart, ‘Measuring Optical Distortion in Aircraft Transparencies: A Fully Automated System for Quantitative Evaluation’, *Machine Vision and Applications*, Vol. 22, pp. 791-804, 2011.
8. U Pingel, ‘New Moiré-Fringe-Method to Inspect Transmitted Distortion and Point-Defects in Sheet-Glass’, *Proceedings Glass Processing Days*, pp. 120-124, September 1997.
9. A S Redner and G K Bhat, ‘Moiré Distortometry for the Quantitative Evaluation of Optical Quality Glass’, *Proceedings Glass Processing Days*, pp. 166-168, June 1999.
10. G E Elsinga, B W van Oudheusden, F Scarano, and D W Watt, ‘Assessment and Application of Quantitative Schlieren Methods: Calibrated Color Schlieren and Background Oriented Schlieren’, *Experiments in Fluids*, Vol. 36, pp. 309-325, 2004.
11. Zygo website description of the Verifire Series of phase-shifting interferometers.  
<http://www.zygo.com/?/met/interferometers/verifire/>







---